Chemical Physics Letters 468 (2009) 23–27

Contents lists available at ScienceDirect

Chemical Physics Letters

journal homepage: www.elsevier.com/locate/cplett

Dissipation effects on laser control of *cis*/*trans* isomerization

Kunihito Hoki, Paul Brumer *

Chemical Physics Theory Group, Department of Chemistry, and Center for Quantum Information and Quantum Control, University of Toronto, 80 St. George Street, Toronto, Canada M5S 3H6

ARTICLE INFO

Article history:
Received 8 February 2008
In final form 18 November 2008
Available online 3 December 2008

ABSTRACT

Photoisomerization in a dissipative environment is examined using optimal control within the secular Redfield approximation. With decoherence assumed rapid compared to relaxation, we find that as the environment-induced dissipation increases the optimal pulse moves towards earlier pulse times (to take advantage of relaxation effects), shorter duration, increased power, with lower resultant target cross sections. The control mechanism is seen to change from pump–dump to pump–dump-plus-environmentally-induced-relaxation as the coupling to the environment increases.

1. Introduction

Significant progress has been made over the past two decades in controlling atomic and molecular processes via laser excitation [1,2]. Such progress has generally been confined to isolated systems, where system coherence is preserved. The situation where control is carried out in an open system, wherein external influences destroy system coherence, is far less well studied in theory (for a recent review see [3]). In this Letter we examine the control of photoinduced *cis*/*trans* isomerization under sample dissipative conditions, a process of widespread significance. Of particular interest is the nature of the control mechanism as a function of the dissipative coupling.

To explore the effects of dissipation on the control of photoisomerization under various dissipative conditions, we consider a 'bare-bones' two-state model for optimal control of *cis*/*trans* isomerization, where the dynamics is treated by means of Redfield theory, within the secular approximation [4]. In this model the system consists of two electronic states, with one nuclear degree of freedom representing the reaction coordinate; all other degrees of freedom are considered as an Ohmic bath. The system and bath couple through a parameter η. The model, albeit limited, has been successful [5] in explaining, for example, the observed control [6] over *trans* to *cis* isomerization of 3,3′-diethyl-2,2′-thiacyanine iodide (NK88) in methanol.

The two-state model, shown in Fig. 1 is regarded as a minimal model system corresponding to isomerization induced by UV lasers, where intra-molecular rotation occurs with respect to a carbon–carbon double bond after photoexcitation. The excited state is generally a few eV above the ground state, and has a higher transition moment (oscillator strength of order $f \sim 1$), than other electronic states. The diabatic ground and excited states show a potential crossing at the transition state, where the intra-molecular rotational angle is 90°.

Dynamics is treated by Redfield theory, a first approximation to the open system, wherein the time evolution of the system experiences a coupling to a Markovian-bath. For numerical stability, we adopt the secular approximation to the Redfield theory. This approach yields system dynamics that quickly loses system electronic and vibrational coherence, consistent with some experimental observations in solution.

Below we consider the nature of the optimal isomerization mechanism for various sample dissipation strengths η. Isomerization is optimized at the 'control time' t_f, here chosen as 500 ps. The system parameters are chosen to create three typical situations, with varying relaxation time T_1 and dephasing time T_2: (a) $\eta = 0$, i.e. no dissipation, so that the relaxation time T_1 is infinite, (b) moderate coupling to the bath, in which the decoherence time $T_2 < t_f$ and $T_1 > t_f$, and (c) strong coupling to the bath, in which $T_2 < t_f$, and $T_1 \approx t_f$. In all cases, $T_1 > T_2$. It should be noted that in the limiting case of $T_1 \ll t_f$ and assuming little tunneling between the *cis* and *trans* configurations, weak and continuous excitation using a one color laser is an efficient mechanism to bring the system from initial *trans* to product *cis*. That is, the system decoheres rapidly after excitation and then relaxes down to both *cis* and *trans*. The *trans* is then re-excited until the vast amount of *trans* is converted to *cis*. A more sophisticated scenario uses a cw version of a pump–dump scenario to drive the isomerization [7].

2. Model and method

Consider a minimal model of photoisomerization consisting of the system with Hamiltonian H_S, the bath H_B, system–bath coupling H_{SB}, and system-electric field coupling described in the dipole approximation. The total Hamiltonian is then given by

$$H = H_S + H_B + H_{SB} - \mu E(t), \tag{1}$$

* Corresponding author. Fax: +1 416 978 5325.
E-mail address: pbrumer@chem.utoronto.ca (P. Brumer).

0009-2614/$ - see front matter © 2008 Elsevier B.V. All rights reserved.
doi:10.1016/j.cplett.2008.11.088

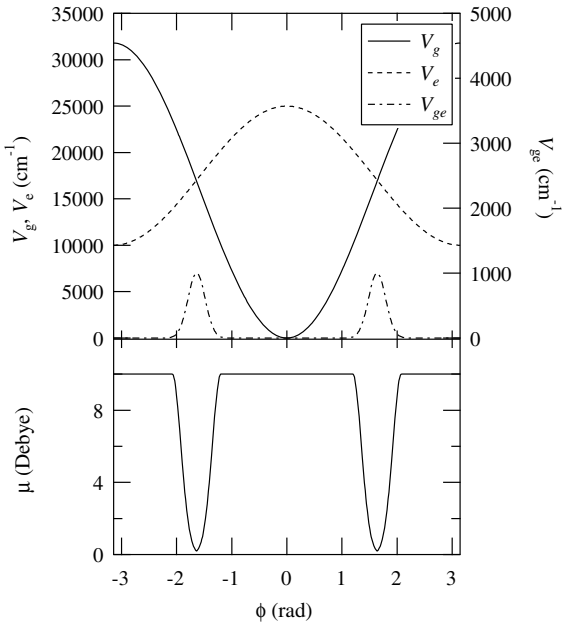

Fig. 1. (top panel) Diabatic potential surfaces V_g and V_e, and potential coupling V_{ge} with respect to reaction coordinate α. The potential has two energy minima, at $\phi = 0$ and π rad, corresponding to the *trans* and *cis* configuration of the molecule, respectively. (bottom panel) The transition dipole moment μ. Here, μ at the *trans* and *cis* configuration is set at $\mu = 10$ Debye.

where H_S describes the isomerization process along a one dimensional reaction coordinate ϕ, H_B represents all other degrees of freedom, μ is the transition dipole moment, and $E(t)$ is the electric field at time t. The eigenvectors and eigenvalues of H_S are denoted $|i\rangle$ and λ_i.

In terms of the two participating electronic states, the system Hamiltonian is given by

$$H_S = \begin{pmatrix} K + V_g(\phi) & V_{ge}(\phi) \\ V_{eg}(\phi) & K + V_e(\phi) \end{pmatrix}, \tag{2}$$

where $K = -\frac{\hbar^2}{2m}\frac{\partial^2}{\partial\phi^2}$ is the kinetic energy, $V_g(\phi)$ and $V_e(\phi)$ are the diabatic potential surfaces of ground and excited electronic state, and $V_{ge}(\phi) = V_{eg}(\phi)$ is the coupling potential between two electronic states (see Fig. 1). In the adiabatic representation the ground state potential is a double well, and each potential well corresponds to the *cis* or *trans* configuration.

In this Letter, we set the effective mass $m = 2.5$ amu Å^2, $V_g(\phi) = A_0(1 - \cos\phi)$, $V_e(\phi) = A_1 + A_2\cos\phi$, $V_{eg}(\phi) = A_3\{g(\phi,\phi_0) + g(\phi,\phi_1)\}$, where A_0, A_1, A_2, A_3, ϕ_0 and ϕ_1 are 15 900 cm^{-1}, 17 500 cm^{-1}, 7500 cm^{-1}, 1000 cm^{-1}, 0.52π rad, and -0.52π rad, respectively. Here, $g(\phi,\phi') = \exp[-(\phi-\phi')^2/0.0049\pi^2]$. The choice of parameters leads to a realistic range of behavior, as seen below.

The transition dipole moment μ is expressed in terms of the two electronic states as

$$\mu = \begin{pmatrix} 0 & \mu_{ge}(\phi) \\ \mu_{eg}(\phi) & 0 \end{pmatrix}, \tag{3}$$

where $\mu_{ge}(\phi) = \mu_{eg}(\phi) = 10(1 - g(\phi,\phi_0) - g(\phi,\phi_1))$ Debye. Our choice of parameters corresponds to an oscillator strength $f \simeq 1$ in the Franck–Condon region of the *trans* configuration.

The bath is described as a set of harmonic oscillators of frequency ω_α

$$H_B = \sum_\alpha \hbar\omega_\alpha b_\alpha^\dagger b_\alpha \tag{4}$$

with system–bath coupling:

$$H_{SB} = Q\sum_\alpha \hbar\kappa_\alpha\left(b_\alpha^\dagger + b_\alpha\right), \tag{5}$$

where $b_\alpha^\dagger$ and b_α are the creation and annihilation operators pertaining to the αth harmonic oscillator. The operator Q is defined as

$$Q = \begin{pmatrix} \cos\phi & 0 \\ 0 & \cos\phi \end{pmatrix}, \tag{6}$$

and the coupling constant κ_α and spectrum of the bath are chosen in accord with an Ohmic spectral density

$$J(\omega) = 2\pi\sum_\alpha \kappa_\alpha^2\delta(\omega - \omega_\alpha) = \eta\omega e^{-\omega/\omega_c}, \tag{7}$$

where the strength of the system–bath coupling is determined by the dimensionless parameter η, and $\omega_c = 450$ cm^{-1}.

The dissipative dynamics of the system is included via the Redfield equation in the secular approximation [4]. Although approximate, we found optimization within the Redfield approach without the secular approximation to be far less stable computationally. Here, the evolution of diagonal elements $\rho_{ii}(t)$ of the system density matrix is given by

$$\frac{\partial}{\partial t}\rho_{ii}(t) = -i\frac{E(t)}{\hbar}\sum_m[\rho_{im}(t)\mu_{mi} - \mu_{im}\rho_{mi}(t)] + \sum_{j\neq i} w_{ij}\rho_{jj}(t) - \rho_{ii}(t)\sum_{j\neq i} w_{ji}. \tag{8}$$

Here, each index denotes a quantum number of the system, including both of the electronic and vibrational degrees of freedom. Note that a state labeled by the quantum number is an eigenstate of the system Hamiltonian H_S including the coupling potential $V_{ge}(\phi)$. In this expression the transition probability is $w_{ji} = \Gamma^+_{ijji} + \Gamma^-_{ijji}$, where

$$\Gamma^+_{ljik} = \frac{1}{\hbar^2}\int_0^\infty d\tau e^{-i\omega_{ik}\tau}\langle H_{SB_{lj}}(\tau)H_{SB_{ik}}\rangle_B \tag{9a}$$

$$\Gamma^-_{ljik} = \frac{1}{\hbar^2}\int_0^\infty d\tau e^{-i\omega_{lj}\tau}\langle H_{SB_{lj}}H_{SB_{ik}}(\tau)\rangle_B. \tag{9b}$$

The quantity $\omega_{ij} = (\lambda_i - \lambda_j)/\hbar$, and the brackets $\langle\ldots\rangle_B$ denote a trace over the bath degrees of freedom with Boltzmann distribution at $T = 300$ K, and $H_{SB_{ij}}(t) = e^{iH_Bt/\hbar}H_{SB_{ij}}e^{-iH_Bt/\hbar}$.

Using Eqs. (5) and (7), Eq. (9) can be rewritten as

$$\Gamma^+_{kijl} = \frac{1}{2\pi}Q_{lj}Q_{ik}\int_0^\infty d\tau\int_0^\infty d\omega J(\omega)\cdot\{[\bar{n}(\omega)+1]e^{-i(\omega_{ik}+\omega)\tau} + \bar{n}(\omega)e^{-i(\omega_{ik}-\omega)\tau}\}, \tag{10}$$

and $\Gamma^-_{ljik} = (\Gamma^+_{kijl})^*$, where $\bar{n}(\omega) = \{\exp(\hbar\omega/k_bT) - 1\}^{-1}$ is the Bose frequency distribution. After some algebra, we obtain

$$w_{ji} = \begin{cases} |Q_{ji}|^2 J(-\omega_{ji})[\bar{n}(-\omega_{ji}) + 1] & \text{for } \omega_{ji} < 0 \\ |Q_{ji}|^2 J(\omega_{ji})\bar{n}(\omega_{ji}) & \text{for } \omega_{ji} > 0 \end{cases} \tag{11}$$

The evolution of the off-diagonal elements is described as

$$\frac{\partial}{\partial t}\rho_{ij}(t) = -i\omega_{ij}\rho_{ij}(t) - \gamma_{ij}\rho_{ij}(t) - i\frac{E(t)}{\hbar}\sum_m[\rho_{im}(t)\mu_{mj} - \mu_{im}\rho_{mj}(t)], \tag{12}$$

with dephasing rate, Reγ_{ij}, and frequency shift, Imγ_{ij}, as

$$\gamma_{ij} = \sum_k\left(\Gamma^+_{ikki} + \Gamma^-_{jkkj}\right) - \Gamma^+_{jjii} - \Gamma^-_{jjii}. \tag{13}$$

The optimal electric field $E(t)$ to make the *cis* configuration from the initial *trans* is designed by maximizing the objective functional

$$O\{t_f, E\} = \mathrm{Tr}[\rho(t_f, E)W] - A\int E(t)^2 dt, \tag{14}$$

where $\rho(t_f, E)$ is a density operator of the system at the target time $t_f = 500$ fs, and W is the target operator, chosen as a projector onto the lowest 14 eigenstates localized around the *cis* configuration.

The second term in Eq. (14) mitigates against large energy in the electric field, corresponding to the numerical technique known as regularization [8]. The weight factor A was adjusted through a numerical optimization procedure so that the ratio of the first to the second term in Eq. (14) is approximately 5:1, stabilizing the computation. The resultant qualitative picture was found to be insensitive to reasonable changes of the ratio, from 10:1 to 2:1. Note that the functional form of $E(t)$ was not restricted. Rather, it was defined on a time grid and allowed any shape. A cw $E(t)$ was used to initiate the optimization algorithm.

The system eigenvectors and eigenvalues $|i\rangle$ and λ_i were calculated by diagonalizing the system Hamiltonian in a sine and cosine basis, with periodic boundary conditions and symmetry at $\phi = 0$ and π imposed on the system. Computation of integrals in Eq. (10) were carried out by a FFT program package. Finally, Eqs. (8) and (12) were numerically integrated using the 4th order Runge–Kutta method. Here, the initial condition $\rho(t = 0)$ is set to a Boltzmann distribution of system eigenstates at 300 K. Furthermore, the electric field that maximizes the objective functional in Eq. (14) was numerically evaluated by a monotonically convergent algorithm [9].

3. Results and discussion

As a first example, consider the case where the system is closed, i.e. the system Hamiltonian H_S is not coupled to the bath, with the strength parameter $\eta = 0$. Fig. 2 shows the optimal pulse and time dependence of the population of the target *cis* product, $P_{cis}(t) = \mathrm{Tr}[\rho(t)W]$. The optimal electric field is seen to consist of two pulses, an earlier pulse of carrier frequency $\sim 25\,000\ \mathrm{cm}^{-1}$ and a later pulse centered on $\sim 10\,000\ \mathrm{cm}^{-1}$. Laser powers are less than $2.5 \times 10^9\ \mathrm{W/cm^2}$.

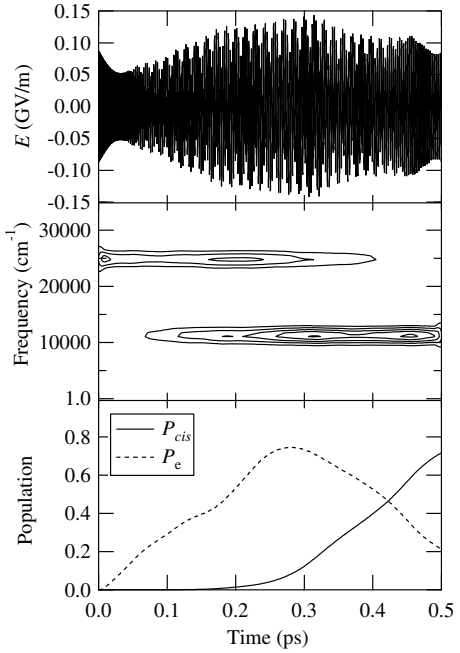

Fig. 2. (top panel) The optimal electric field $E(t)$ with $\eta = 0$. Note that 1 GV/m corresponds to a power of $\approx 2.5 \times 10^{11}\ \mathrm{W/cm^2}$. (middle panel) Time–frequency resolved spectrum. (bottom panel) The time propagation of *cis* population P_{cis} and excited population P_e.

The 25 000 cm^{-1} centered pulse corresponds to the Franck–Condon excitation of the initial *trans* molecule. At $t = 250$ fs, 75% of initial density has been transferred to several eigenstates that have energy $\sim 25\,000\ \mathrm{cm}^{-1}$ above the potential energy minimum. The second pulse deexcites the system to vibrationally excited *cis* states of energy $\sim 15\,000\ \mathrm{cm}^{-1}$. In this case the pump and dump process have enough energy resolution to selectively drive population from initial *trans* to vibrationally excited *cis*. Note that vibrationally excited *trans* is barely created by the dump pulse at the target time, as evidenced by the fact that $P_e + P_{cis} \sim 1$. This is quite distinct from the results for the dissipative cases below, where vibrationally excited *trans* is created along with the *cis* product.

Hence, the optimal mechanism under the indicated decoherence-free conditions is a Tannor-Rice pump–dump mechanism [10,11]. As is typical in these circumstances, the relative phases of the pump and dump pulses do not affect the control.

Consider now the case where the system interacts with a bath. Fig. 3 shows results for moderate strength parameter $\eta = 2$. Given this value, the bare electronic dephasing time around the Franck–Condon region of the *trans* configuration is ~ 40 fs. Here, the bare electronic dephasing time denotes the time for bath induced dephasing of two eigenstates of the system Hamiltonian, the first being the lowest ground eigenstate and the second being the state, primarily on the upper electronic surface, that has the largest transition amplitude with the ground state. With $\eta = 2$, energy relaxation from the excited state to the *cis* target does not occur within the target time of $t_f = 500$ fs.

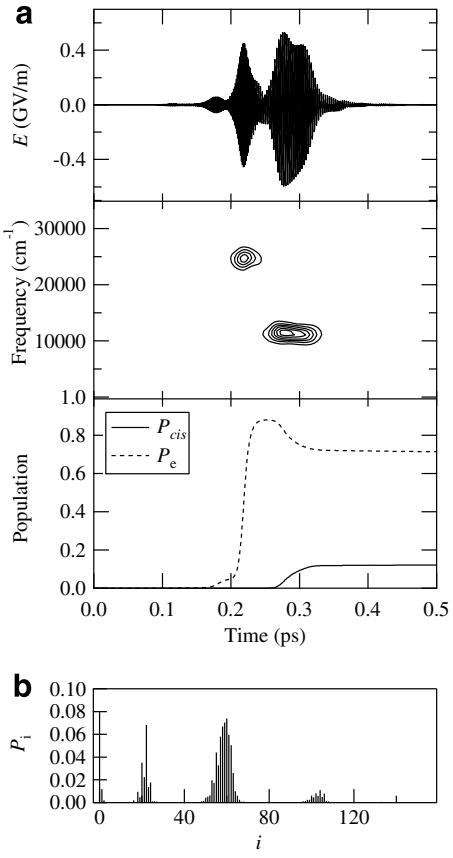

Fig. 3. Optimal control results with $\eta = 2$. (a) (top panel) The optimal electric field $E(t)$. (middle panel) Time–frequency resolved spectrum. (bottom panel) The time propagation of *cis* population P_{cis} and excited population P_e. (b) Population of eigenstates at $t = 0.35$ ps. Here, populations of 160 symmetric eigenstates with respect to $\phi = 0$ and π are shown. States around $i \sim 20$ correspond to vibrationally excited *cis* and *trans*, ~60 corresponds to electronically excited *trans*, and ~100 corresponds to electronically excited *cis*.

As in the $\eta = 0$ case, the electric field is seen to consist of two pulses, the earlier pulse (at 200 fs) with carrier frequency of 25 000 cm^{-1} and the later pulse centered around 280 fs and 10 000 cm^{-1}. However, by contrast with the $\eta = 0$ case, the maximum intensity of the field is 16 times larger, and the pulses are far more localized in time. Indeed, the time duration of the first pulse is seen to be shorter than the bare electronic dephasing time of 40 fs, the shorter stronger pulse exciting the molecule more efficiently under the dissipative condition.

After the pump pulse, ~90% of density is excited. Immediately after excitation the vibrational states on the upper electronic state, of which the excited wavepacket is composed, dephase due to interaction with the bath, and the wavepacket becomes a diffuse incoherent collection of eigenstates. The timescale for this vibrational dephasing is on the same order as that of the bare electronic dephasing. By $t \sim 280$ fs, the mixed-state density on the upper surface reaches the *cis* configuration. The dump pulse then begins to drive population down to the product *cis*.

Fig. 3 also shows that the second pulse is similarly localized in time; the field terminates at $t \sim 350$ fs. Because of the high intensity of the pulses and rapid loss of phase between system states, the pump–dump pulse sequence does not have enough selectivity to bring the system effectively to the *cis* target. The results show that after the dump process, density has been transferred to vibrationally excited states of both *trans* and *cis*, and electronically excited *cis*. After the dump pulse at $t \sim 0.35$ ps, the three population components that do not correspond to *cis* product, (i.e. the initial *trans*, the vibrationally excited *trans*, and the electronically excited *cis*), no longer change (see Fig. 3b). Since there are no phase relationships amongst the three components and the target, further attempts to preferentially enhance the *cis* target by using laser pulses is difficult.

In this $\eta = 2$ case, the designed pulses are seen to be shorter and more intense than in the dissipative free case ($\eta = 0$). The optimal mechanism is seen to complete each of the pump and dump processes within the bare electronic dephasing time of ~40 fs, The net result is that the selectivity of population transfer is poor; 75% of the density is transferred to non-target states or stays in the initial *trans* configuration. Hence, in contrast with the first example, $P_{cis}(t)$ is only 15%. Hence, dissipation significantly reduces the ability to control the photoisomerization process.

Fig. 4 shows the third case, in which the coupling parameter is increased to $\eta = 15$. Given this parameter, the bare electronic dephasing time around the Franck–Condon region of the *trans* configuration is ~5 fs, and relaxation from excited *trans* to target *cis* occurs within $t_f = 500$ fs. The optimal electric field is now seen to consist of three pulses, the first pulse has a carrier frequency at ~ 25 000 cm^{-1}, the second at ~ 10 000 cm^{-1}, and the third has a central frequency of ~ 20 000 cm^{-1}. These frequencies correspond to energy differences between the initial *trans* and electronically excited *trans*, the excited *trans* and target *cis*, and electronically excited *cis* and target *cis*, respectively. The pulses are more intense and shorter than the second case, in response to the strong dissipative conditions in the system. Also, in this case, the optimal electric field shows a third pulse that transfers electronically excited *cis* molecules to vibrationally excited *cis*molecules on the lower electronic state. In contrast with the second example, the pulse sequence operates only at short times relative to the control time t_f and then relies upon the energy relaxation from excited state to vibrationally excited *cis* to help form the *cis* product. This is evidenced by the slow falloff in P_e in Fig. 3 after ~ 100 fs. Note that this relaxation process does not produce the target state selectively. Rather, the short and intense first pulse has a wide energy width, producing an excited state consisting of many vibrationally excited states. The fast decoherence then produces a state devoid of coherence. Hence, the subsequent relaxation branches incoherently into the *cis* and *trans* states. The branching ratio at that time depends only on the system Hamiltonian and system–bath coupling, but does not depend on the electric field. Note that in this case the field also tries selective de-excitation into the target *cis* by means of dump pulses. However, selective population transfer here is even harder than in the second case.

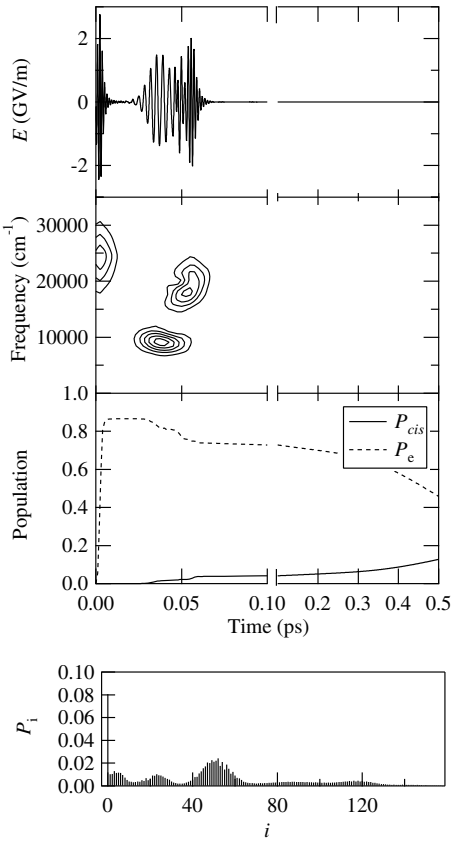

Fig. 4. Optimal control results with $\eta = 15$. (a) (top panel) The optimal electric field $E(t)$. (middle panel) Time–frequency resolved spectrum. (bottom panel) The time propagation of *cis* population P_{cis} and excited population P_e. (b) Population of eigenstates at $t = 80$ fs. Here, only 160 of symmetric eigenstates with respect to $\phi = 0$ and π are shown for the sake of appearance. States around $i \sim 20$ corresponds to vibrationally excited *cis* and *trans*, ~60 corresponds to electronically excited *trans*, and ~100 corresponds to electronically excited *cis*.

Fig. 4b shows the population of system eigenstates at $t = 80$ fs. At this time, the pump–dump pulse sequence has just ended, and the relaxation produce follows until $t = 0.5$ ps. In the figure, the population is seen to be spread over 200 eigenstates (including symmetric and anti-symmetric eigenstates), where the vibrationally excited states and electronically excited states have no coherence. The resultant pulse sequence is only capable of producing 4% of the target state, and the total target yield after the subsequent relaxation processes is 13%.

4. Summary

Manipulating molecular processes in open systems remains one of the major challenges in quantum control (see, e.g. [12]). We have examined optimal control of *cis*/*trans* isomerization via a two-state model, within Redfield theory with secular approximation.

Optimal mechanisms of isomerization under no, moderate and strong dissipative conditions are discussed. In all cases, selective control of *cis*/*trans* isomerization was found to result from a

pump–dump pulse sequence. However, the strength of dissipation on the system strongly affects the shape of the pulses. In cases with nonzero dephasing times, the optimal electric field has a shorter pulse duration than the electronic dephasing time. Selective population transfer into target *cis* was carried out by tuning the frequency of the pulses and coherence between pulses does not play an important role. The optimal mechanism loses the target selectivity as the dissipation effect on the system becomes strong. That is, due to the system–bath coupling, the photoexcited system relaxes into both lower energy state *cis* and *trans*. Further, since the electronic and vibrational excited state loses coherence when it relaxes, due to the nature of Redfield theory in the secular approximation, the branching ratio between *cis* and *trans* does not depend on coherence of the system states after the pulse excitation.

The nature of the exact system eigenstates provides insight into the observed results. Specifically, from the diabatic states perspective, the total system eigenstates in the energy regime of the *cis* product span the full $-\pi \leqslant \phi \leqslant \pi$ range. Hence, de-excitation to such states produces both the *cis* and *trans* vibrationally excited product. As a result, in the absence of coherence, lost due to the interaction with the bath, it is difficult to preferentially produce the *cis* product.

One further note is in order. As in all optimal control studies, the details of the observed optimal result are intimately dependent upon the constraints set in the simulation. The qualitative features are, however, expected to be generic.

References

[1] M. Shapiro, P. Brumer, Principles of the Quantum Control of Molecular Processes, Wiley, New York, 2003.
[2] S.A. Rice, M. Zhao, Optical Control of Molecular Dynamics, Wiley Interscience, New York, 2000.
[3] P. Nuernberger, G. Vogt, T. Brixner, G. Gerber, PCCP 9 (2007) 2470.
[4] K. Blum, Density Matrix Theory and Applications, Plenum Press, New York, 1981.
[5] K. Hoki, P. Brumer, Phys. Rev. Lett. 95 (2005) 168305.
[6] G. Vogt, G. Krampert, P. Niklaus, G. Gerber, Phys. Rev. Lett. 94 (2005) 068305.
[7] D. Gruner, M. Shapiro, P. Brumer, J. Phys. Chem. 96 (1992) 281.
[8] H. Engl, M. Hanke, A. Neubauer, Regularization of Inverse Problems, Series: Mathematics and its Applications, vol. 375, Springer, 1996.
[9] Y. Ohtsuki, W. Zhu, H. Rabitz, J. Chem. Phys. 110 (1999) 9825.
[10] D.J. Tannor, S.A. Rice, J. Chem. Phys. 83 (1985) 5013.
[11] T. Seideman, M. Shapiro, P. Brumer, J. Chem. Phys. 90 (1989) 7132.
[12] L.-A. Wu, A. Bharioke, P. Brumer, J. Chem. Phys. 129 (2008) 041105.